09

Development of a waveguide superconducting detector with photon number resolution

© I.O. Venediktov,[1,2] V.V. Kovaluk,[1,2] P.P. An,[2,3] E.D. Sheveleva,[2,3] E.M. Baeva,[1,3] Z.M. Dashevsky,[4] R. Shnek,[4] G.N. Goltsman[1,5]

[1] National Research University Higher School of Economics,
109028 Moscow, Russia
[2]National University of Science and Technology MISiS,
119049 Moscow, Russia
[3]Moscow Pedagogical State University,
119991 Moscow, Russia
[4]School of Electrical and Computer Engineering, Ben-Gurion University,
84105 Beersheba, Israel
[5]Russian Quantum Center,
121205 Moscow, Russia
e-mail: ilia1999ven@gmail.com

Received April 26, 2024
Revised April 26, 2024
Accepted April 26, 2024

This work presents a superconducting single-photon detector with photon number resolution based on integrated optics on a silicon nitride platform for a wavelength of 914 nm. The detector is based on a space-time multiplexing scheme and consists of a plurality of pixel detectors connected in series by a microstrip line, which acts as a delay line and an impedance transformer. The work describes the fabrication route of the detector, the calculation of the electrical part of the detector, the influence of the number of detectors on the dynamic range of the resolution of the number of photons is assessed, and the experimental values of the critical temperature and critical current of the detector are obtained. The results of this work can be used in the design of scalable quantum optical microcircuits for ion and photon computers.

Keywords: integrated optics, superconductivity, single-photon detector, quantum optics.

DOI: 10.61011/TP.2024.07.58813.127-24

Introduction

Single-photon detectors (SPD) [1] play an important role in the development of quantum computations, quantum communications and metrology. An ideal single-photon detector shall have a unit quantum efficiency, small dark counts, high counting rate, low jitter and wide dynamic photon number resolution range and high photon number resolution accuracy [1]. Among all types of single-photon detectors, superconducting detectors have record-breaking specifications that are necessary for quantum optical operations.

Transition edge sensors (TES) [2–6] and microwave kinetic inductance detectors (MKID) [7,8] have high quantum efficiency, low dark count level and photon number resolution capability. In case of TES, the photon number resolution capability is explained by the dependence of resistance variation on incedent optical power. In case of MKID, the inductance variation depends on the incident power resulting in the resonance curve shift by which the optical power and, consequently, the photon number may be determined. However, these detectors have low counting rate (~ 1 MHz), high jitter (nanosecond level) and extremely low operating temperature (~ 100 mK) [9].

On the contrary, the superconducting nanowire single photon detectors (SNSPDs) have a quantum efficiency close to unity [10,11], GHz counting rate [12], picosecond-level jitter [13], subhertz darl count level [14] and a relatively high operating temperature (2−4 K). Despite all these advantages, SNSPD itself has no photon number resolution capability and has threshold behavior. Improved circuit schemes of SNSPD were shown to resolve the photon number using transition coplanar lines for impedance matching [15] and broadband low-temperature amplifiers [16], but such circuits are limited by 3 to 4 photon resolution.

Another way to build a photon number resolution (PNR) SNSPD is to group several detector sections connected in parallel or in series into an array through resistors [17–22]. In this case, when detector sections are actuated, pulses from them are summed up and pulses proportional to the number of absorbed photons are recorded at the circuit output. Though such circuits allow a 24 photon resolution to be achieved [20], they have a set of significant disadvantages. First, to reduce the probability that several photons hit the detector, the number of sections shall be much higher than the photon number. Second, the efficiency of detecting several photons (N) is an power function of single photon efficiency $\eta(1)^{(N)}$.

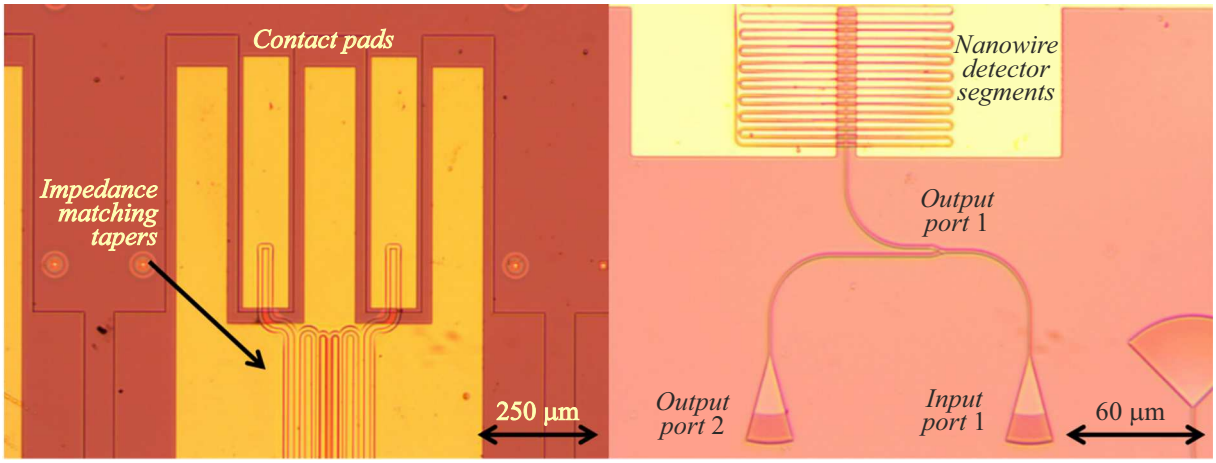

Figure 1. Microphotographs of the fabricated detector.

A new approach to build a waveguide PNR SNSPD is a spatiotemporal multiplexing circuit [23] that is used to resolve photon number in a pulse and spatial detector actuation position to achieve the 100 photon resolution. Due to such dynamic photon number resolution range, it was possible study the statistics of photons from a coherent and thermal source and to calculate the correlation functions $g^n(0)$ of these sources up to the 15th order. The coherent source had the Poisson distribution of photon number. The thermal source had the Bose–Einstein distribution with short optical pulse duration and Poisson distribution with long pulse duration. The circuit proposed herein is easily scalable, has a wide photon number dynamic range and is the most promising among all PNR circuits described above. At this point, it has been demonstrated only for the telecommunication wavelength band ($1.55\,\mu$m). The study demonstrates the performance computation of a waveguide PNR SNSPD with a spatiotemporal multiplexing circuit for a wavelength of 914 nm on which GaAs quantum dots (910–925 nm) generate photons whose radiation statistics is described by the sub-Poisson distribution [24]. Such dots currently have a low second-order correlation function $g^2(0)$, high degree of indistinguishability and compact design and, thus, are promising candidates for integration together with single-photon detectors and logical elements for a scalable chip-based computer.

1. Description of the device

The devices of interest were made on a Si_3N_4substrate covered with a NbN layer. The Si substrate thickness is $525\,\mu$m, SiO layer thickness is$_2$ $2.5\,\mu$m, waveguide layer thickness is Si_3N_4 220 nm (etching depth of 110 nm) and NbN thickness is about 5 nm. To form a ground contact of the microstrip line, the chip was covered with a 200 nm silicon oxide layer and a 300 nm gold layer, and an impedance transformer in the form of Klopfenstein tapers was used to match the detector impedances with the measuring electronics [25]. The typical device (Figure 1) consisted of a Y-splitter (50 : 50) and 2 focusing diffraction gratings optimized for a wavelength of 914 nm.

Port *1* was used for radiation input, port *2* was used as a calibration port. The remaining splitter port outputs the optical power to the waveguide detector — a long NbN nanostrip that intersects the waveguide transversely several times. Each intersection between the nanostrip and waveguide is a separate detector pixel that may absorb a photon with some probability depending on the pixel geometry and on the physical properties of the nanostrip and waveguide material. When a photon with energy $h\upsilon > 2\Delta$, where Δ is the superconductor energy gap at a given temperature, is absorbed by a pixel, local disintegration of the Copper pairs occurs and high-energy quasiparticles are formed. As a result, hot spot is formed during thermalization. After completion of the thermalization, diffusion of hot electrons from the hot spot area takes place resulting in expansion of the spot. When the hot spot expands, bias current fed to the detector is displaced from it to the nanostrip edges resulting in the growthof current density in these areas. When the current density exceeds the critical level, an area across the strip changes to the resistive state. This gives rise to 2 voltage pulses: positive and negative pulses that propagate in opposite directions. Since all pixels are connected in series through the delay lines, these pulses are time spaced (time multiplexing). The arriving number of electric pulses (positive or negative) defines the number of photons in the optical pulse, and the pulse arrival time is used to determine the actuated detector position. The photon number resolution is achieved due to multiple detectors arranged sequentially series such that the absorption probability of an individual detector is low, but due to a large number of detectors, the total detection efficiency may be close to unity. Since the probability of absorption of a single photon by a single pixel detector is low, then the probability of multiphoton absorption events in the next pixels declines exponentially. Thus, a situation may

be achieved when all photons are absorbed mainly through the single-photon absorption events, and the number of electric pulses may be used to estimate the number of input optical photons.

2. Electrical design of the detector

When a photon is absorbed by a NbN superconductor strip, 2 pulses with opposite polarity occur and propagate in the opposite directions via the microstrip line. The strip impedance in the area where the absorption occurs is about several kΩ, whereas the measuring electronics impedance is 50 Ω. Due to the impedance mismatch, the voltage pulse is reflected resulting in signal amplitude reduction and in subsequent re-reflections that may be taken or false actuations (afterpulses). For impedance matching, we used the Klopfenstein taper topology [25] to perform smooth (adiabatic) matching between the active detector area and the output circuit. In case of integrated circuit, we varied the taper width for smooth impedance variation. Dependence of the impedance on geometrical parameters of the microstrip line is described by the following equations:

$$C = 1.2\varepsilon\varepsilon_0(h + w)/(h - t), \quad w/h < 2, \tag{1}$$

$$C = 1.2\varepsilon\varepsilon_0(h + w - t)/(w - t), \quad w/h \geq 2, \tag{2}$$

where C is the capacity per unit length, ε_0 is the dielectric constant, ε is the dielectric layer permittivity, h is the dielectric layer, w is the nanostrip width, t is the nanostrip thickness, Z is the line impedance, L_s is the nanostrip inductance per square.

Using expressions (1) and (2), we converted the calculated impedances into the nanowire width. The microstrip line parameters in our topology were as follows: initial nanostrip width $w_1 = 0.3\,\mu$m, final width $w_2 = 12.65\,\mu$m, dielectric thickness $h = 220$ nm, with silicon oxide permittivity $\varepsilon = 4$ and NbN film thickness $t = 5$ nm with the initial resistance after photon absorption 1645.5 kΩ.

Since the multiplexing circuit is based on time spacing of signals from different detectors, the detector shall have a necessary parameter — the velocity of electric signal propagation in a microstrip line (v) that may be found according to inductance (L) and capacity (C) per unit length [26]:

$$v = 1\sqrt{LC}. \tag{3}$$

The pulse delay time between the actuated detectors will be defined by the length of a nanostrip connecting them in series. The delay shall be not shorter than the detector jitter time in order to distinguish the pulses from different detectors. The propagation velocity may vary by varying the dielectric thickness and permittivity. In our detector, the minimum distance between the detectors is 200μm, velocity at a width of 300 nm is equal to 2% of the speed of light, thus, the delay time is equal to 33 ps, which is comparable with the SSPD (superconducting single photon detector) jitter. To achieve a better time resolution, the delay time may be increased to 1 ns, which is comparable with the dead time of detector. For this, a delay line of 6 mm in length shall be used. The propagation rate may be reduced by varying the dielectric geometry and permittivity.

Figure 2, *a* shows the dependence of the signal propagation rate on the dielectric thickness $v(h)$ ($w = 300$ nm, $\varepsilon = 4$ and $t = 5$ nm). The curve shows that the propagation velocity v increases with the dielectric thickness, therefore this layer shall be as thin as possible to increase the delay time between signals from different pixel detectors. But such approach has limitations because the waveguide has a finite thickness and the dielectric thickness h cannot be smaller than the waveguide etching depth because this will result in breakdown of the dielectric layer under the waveguide. Usage of a material with higher ε is another approach. Figure 2, *b* shows the dependence of the signal propagation velocity on the buffer layer permittivity of the microstrip line ($w = 300$ nm, $h = 220$ nm, $t = 5$ nm). The curve shows that the propagation velocity decreases as ε increases, therefore more optically dense materials with high ε may be used to reduce the propagation velocity. All calculations were made for a width of $w = 300$ nm because only the areas with such thickness (where photon absorption takes place) give the time delay of pulses between pixels. Tapers with a variable width are placed symmetrically and therefore will not give any time delay. However, the taper length may affect the line cutoff frequency because the Klopfenstein taper topology is a low frequency filter. Therefore, these tapers shall be as long as possible to reduce the cutoff frequency and signal reflection from the detector, which in turn may increase the total line inductance and result in the detector pulse drop time.

3. Dependence of the detection efficiency on the number of pixels

The effect of the number of pixels on the photonnumber resolution dynamic range of the detector is important. When a light pulse propagates through a pixel, a part of photons is absorbed with a probability of p, and each photon is absorbed individually. Therefore each pixel detector may be assumed as a beam splitter with splitting ratio p. Using this model together with the Poisson distribution of the photon number, it may be shown that, when there was a state with a mean photon number per pulse n at the detector input, then after propagation of one pixel, it will be also the Poisson state, but with a mean number $n(1 - p)$. The number of photons absorbed by one pixel is np. Thus, the total efficiency of detectors η with$k$-pixels will be

$$\eta = 1 - (1 - p)^k. \tag{4}$$

The efficiency calculated using equation (4) shows the probability of photon absorption after propagation of all pixels and does not describe the dynamic PNR range because absorption may take place through multiphoton events that will result in a lower number of pixel actuations

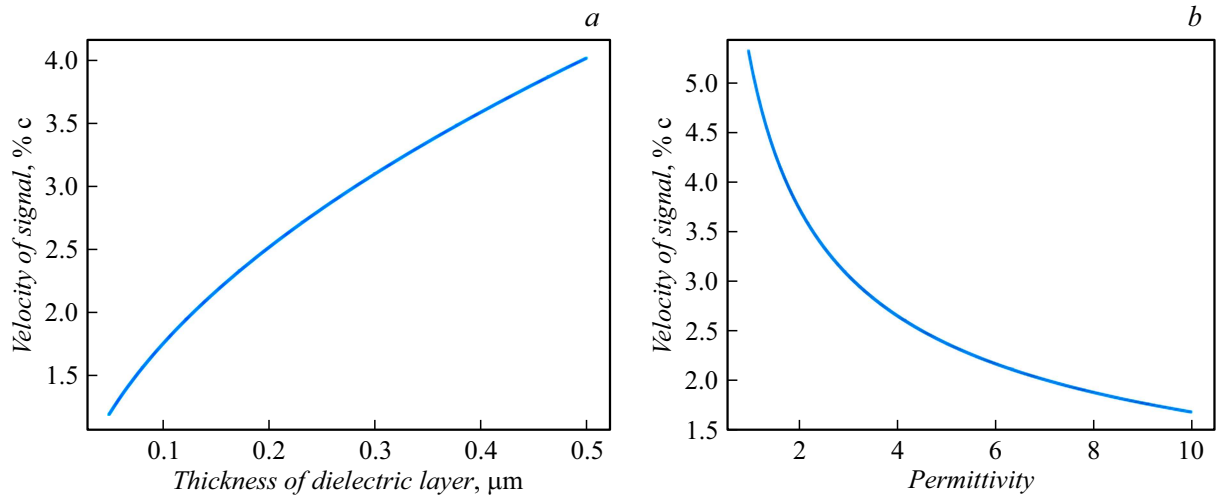

Figure 2. *a* is the dependence of the electric signal propagation velocity on the dielectric layer thickness; *b* is the dependence of the signal propagation rate on the dielectric layer permittivity.

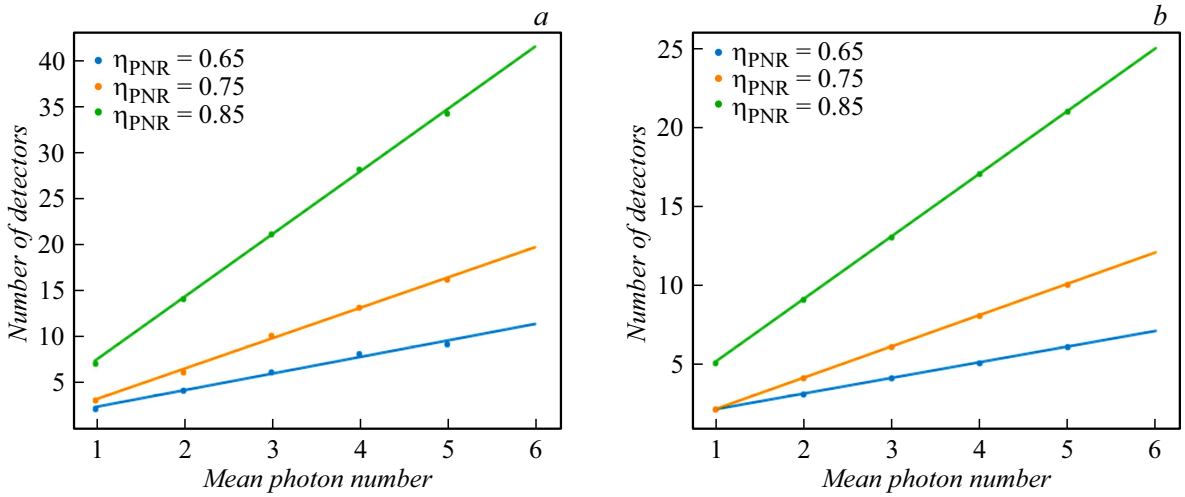

Figure 3. Dependence of the number of detectors to achieve the necessary efficiency of photon number resolution at various mean photon numbers per pulse: *a* — the same detectors; *b* — optimized detectors.

which defines the measured photon number. Then the efficiency in terms of the photon number resolution may be defined as a relation between the mean number of actuations on all pixel detectors and the mean number of photons per pulse.

$$n_l = n_0(1-p)^l, \tag{5}$$

$$\eta_{PNR} = \sum_{i=1}^{n} \left(1 - e^{-n_{i-1}p}\right) / n_0, \tag{6}$$

where n_l is the mean photon number per pulse after propagation of l-pixels, n_0 is the initial photon number per pulse, η_{PNR} is the PNR-efficiency of the detector, p is the absorption probability of the pixel detector.

The equation shows that as the mean photon number per pulse increases and the pixel number remains unchanged, η_{PNR} will decrease. Figure 3, *a* shows the dependence of the pixel number necessary to achieve the set η_{PNR} on the mean photon number per pulse, the total detector efficiency η used for the calculation is equal to 95%.

The curve shows that the dependence of the number of detectors on the mean photon number per pulse is linear which indicates good scalability of the proposed circuit. This circuit may be optimized, if the photon absorption probabilities are varied adaptively on different detectors. The absorption probability may be varied by varying the pixel geometry. Figure 4, *b* shows the pixel topology where absorption depends on the pixel length in contrast to the topology in Figure 4, *a*, where the absorption probability is the same. Thus, the required absorption probability may be achieved by varying the pixel length.

The main idea of optimization is in choosing such absorption probabilities at which each detector would absorb the

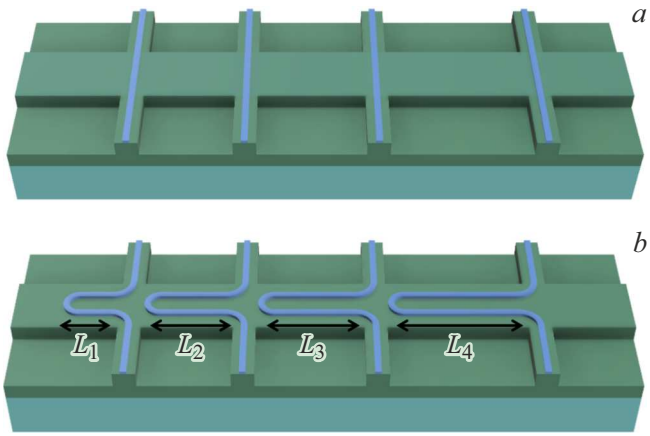

Figure 4. *a* — detector topology with constant probability of absorption on a pixel, *b* — detector topology with variable probability of absorption on a pixel.

same optical power. For this, the absorption probabilities p_i shall vary in accordance with expressions:

$$p_0 = \eta/n, \tag{7}$$

$$p_{i+1} = p_i/(1 - p_i), \tag{8}$$

where n is the total pixel detector number, p_i is the absorption probability at the i-th pixel, η is the total quantum efficiency of the detector.

The curve (Figure 3, *b*) shows the dependence of the pixel number for the achievement of the set η_{PNR} on the mean photon number per pulse for the optimized absorption probabilities. The curve shows that the number of detectors also depends linearly on the mean photon number, but now the number of detectors necessary for the achievement of the required efficiency is approximately 1.5 times as low.

4. Process route

The waveguide PNR detector fabrication process route included several stages.

At stage 1, a 5−7 nm NbN layer deposition to a Si substrate was done. The layer deposition was done by the magnetron sputtering method followed by covering with a 2 nm silicon layer.

Stage 2 used the lift-off photolithography method to form Ti/Au alignment marks (5/80 nm in thickness, respectively).

Stage 3 used the electron-beam lithography on EBPG5000 Raith tool and the plasma-chemical etching in SF_6 : Ar to make nanostrips and NbN tapers.

Stage 4 used the electron-beam lithography on EBPG5000 Raith tool and plasma-chemical etching ($SF6 : CHF_3$) to make the waveguide system of the detector with parameters similar to those used to form the NbN topology.

Stage 5 included preparation by the lift-off photolithography method and formation of dielectric SiO_2 layer above each detector by the electron-beam sputtering method.

The detector fabrication process was completed by formation of the upper ground and lower signal contact pads by the lift-off photolithography with electron-beam sputtering of 5/80 nm Ti/Au.

5. Analysis of the optical system of the detector

Input of the optical radiation into the waveguide via which it enters the detector is an important issue. As the input elements, we used the focusing diffraction gratings the main parameters of which were the period and fill factor. The grating period means the distances between the neighboring grating elements, and the fill factor means the fraction of the period filled with the waveguide material. To find the optimum values of these parameters for 914 nm radiation input, a variation matrix was made with the period varied from 0.68 to 0.72 μm and the fill factor varied from 0.5 to 0.8. For the measurements, the chip with the prepared devices was placed on a table with piezopositioners moving along the x, y, z axes and rotating about the z axis. The table was also equipped with the Peltier element for thermal stabilization within $\pm 0.05^\circ$C. The radiation was input and output using a fiber array placed at an angle of8° to normal. The experimental setup is shown in Figure 5.

The laser radiation was introduced to port *1* (Figure 6, *a*) and the output power was measured from port *2*, and the propagation loss was assumed as negligible. The 914 nm laser was used as the source. Input efficiency per diffraction grating (Figure 6, *b*) η_{in} was calculated using the following equation

$$\eta_{in} = \sqrt{P_{out}/P_{in}}, \tag{9}$$

where P_{out} is the output power from the structure, P_{in} is the input power.

The measurements are shown in Figure 7. The color map shows that the efficiency peak corresponds to: a period of 0.68 μm and a fill factor of 0.56. The maximum efficiency corresponding to these parameters is 10%. The measured efficiency may be used to estimate the power on the detector, which is necessary to estimate its chip-based detection efficiency (without considering the optical input loss).

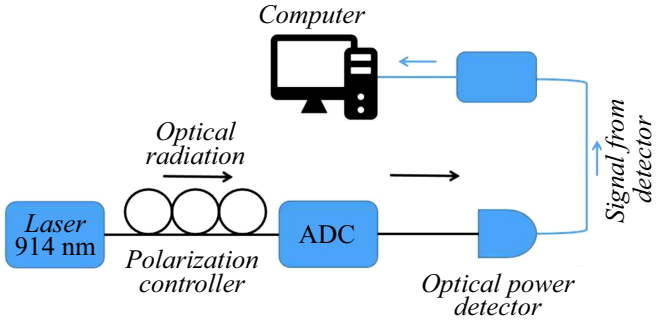

Figure 5. Experimental setup for measurement of input efficiency of focusing diffraction gratings.

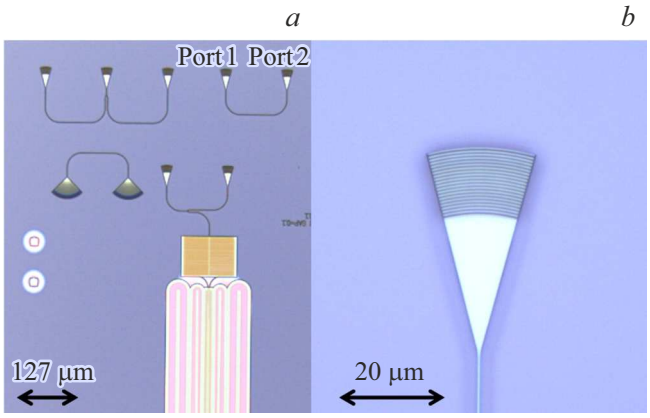

Figure 6. *a* — microphotograph of the waveguide system of the fabricated structure; *b* — magnified image of the focusing diffraction grating.

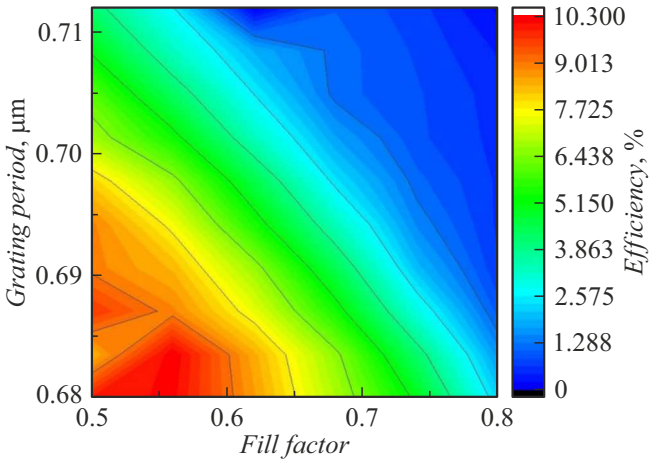

Figure 7. Dependence of the radiation input efficiency on the grating period and fill factor.

Further investigation of the waveguide system of the detector will be devoted to cross-waveguides that form a basis of the pixel detectors due to the estimate of possible loss on them to improve their geometry. Geometry of splitters used to deliver radiation to the detector may be also improved to reduce the light scattering on the detector.

6. Experimental DC measurements

To study the detector characteristics, the the chip with detector attached to a cryogenic dip stick were immersed into the Dewar vessel with liquid helium. A temperature sensor and electric inputs and outputs were placed on the dip stick with the specimen to supply voltage or current to the specimen. Measurements were made using a quasi 4-point configuration. The detector was biased by current from Yokogawa GS200 source in current stabilization mode, voltage was measured by Keysight 34461A voltmeter. Resistance was measured at 50 nA when inserting the mockup slowly into the Dewar vessel resulting in temperature decrease. The resistance vs. temperature curve is shown in Figure 8, *a*. The curve shows that the critical temperature is 8 K. After specimen cooldown to 4 K, the specimen's current-voltage curve was measured in forward and reverse directions (Figure 8, *b*). The obtained critical current was 4 μA making it possible to proceed to the next stage of experimental study: measurement of the detection efficiency and photon number that may be resolved by the detector.

Conclusion

Design methods are described for a waveguide superconductor single-photon number resolution detector for operation at a wavelength of 914 nm. Detector's fabrication route and electrical curcuit design of the detector are reported, dependence of the electric pulse propagation velocity on the microstrip line geometry was shown. The pixel number

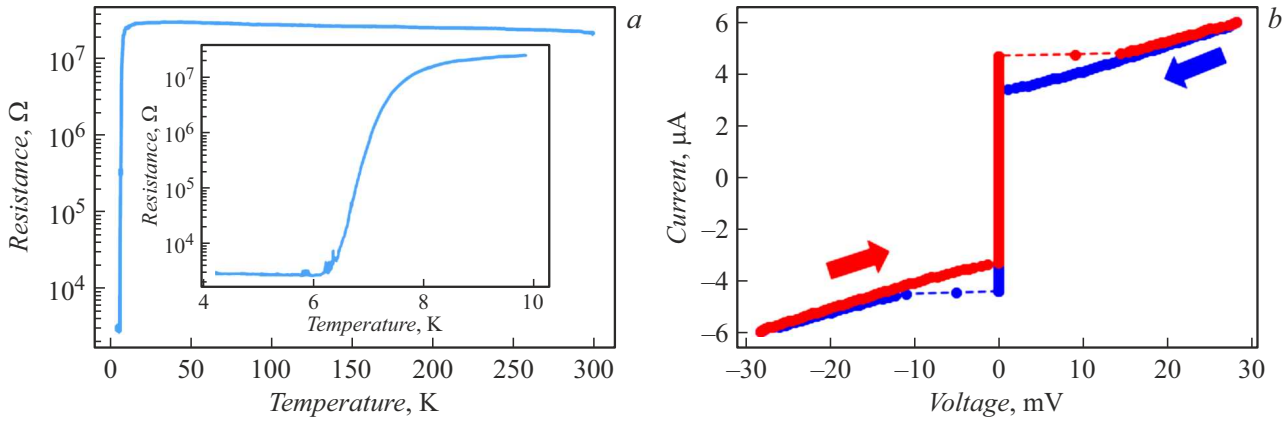

Figure 8. *a* — dependence of the detector resistance on temperature; *b* — current-voltage curve of the detector in forward (red) and reverse (blue) directions.

effect on the detector resolution was estimated numerically and an optimum pixel distribution method was described to reduce the number of detectors without reducing the total detection efficiency. Critical temperature and critical current were obtained experimentally for the fabricated detector and were equal to 8 K and 4 μA, respectively, and the period and fill factor of the grating coupling element were found for operation at a radiation wavelength of GaAs quantum dots (914 nm). Future study will be devoted to increase the critical current of the device, experimental estimation of the detection efficiency and dynamic photon detection range, and optimization of the cross-waveguide and splitter geometry in order to reduce the optical radiation scattering loss.

Funding

The study was supported by State Corporation „Rosatom“ under the Quantum Computation Roadmap (Agreement № 868-1.3-15/15-2021 as of 05.10.2021 and Agreements № P2178, P2179 and P2362) and within the project of university participation into the development of high-technology industry supported by the Ministry of Science and Higher Education of the Russian Federation (Agreement as of 06.04.2022 № 075-11-2022-026).

Conflict of interest

The authors declare that they have no conflict of interest.

References

[1] G.N. Gol'tsman, O. Okunev, G. Chulkova, A. Lipatov, A. Semenov, K. Smirnov, B. Voronov, A. Dzardanov, C. Williams, R. Sobolewski. Appl. Phys. Lett., **79** (6), 705 (2001). https://doi.org/10.1063/1.1388868

[2] A.J. Miller, Sae Woo Nam, J.M. Martinis, A.V. Sergienko. Appl. Phys. Lett., **83** (4), 791 (2003). DOI: 10.1063/1.1596723

[3] A.E. Lita, A.J. Miller, S.W. Nam. Optics Express, **16** (5), 3032 (2008). DOI: 10.1364/OE.16.003032

[4] Th. Gerrits, N. Thomas-Peter, J.C. Gates, A.E. Lita, B.J. Metcalf, B. Calkins, N.A. Tomlin, A.E. Fox, A. Lamas-Linares, J.B. Spring, N.K. Langford, R.P. Mirin, P.G.R. Smith, I.A. Walmsley, S.W. Nam. Phys. Rev. A, **84** (6), 060301 (2011). https://doi.org/10.1103/PhysRevA.84.060301

[5] B. Calkins, P. Mennea, A. Lita, B.J. Metcalf, W.S. Kolthammer, A. Lamas-Linares, J.B. Spring, P.C. Humphreys, R.P. Mirin, J.C. Gates, P.G.R. Smith, I.A. Walmsley, Th. Gerrits, S.W. Nam. Opt. Express, **21** (19), 22657 (2013). DOI: 10.1364/OE.21.022657

[6] M. Eaton, A. Hossameldin, R.J. Birrittella, P.M. Alsing, Ch.C. Gerry, H. Dong, Ch. Cuevas, O. Pfister. arXiv preprint arXiv:2205.01221 (2022).

[7] W. Guo, X. Liu, Y. Wang, Q. Wei, L.F. Wei, J. Hubmayr, J. Fowler, J. Ullom, L. Vale, M.R. Vissers, J. Gao. Appl. Phys. Lett., **110** (21), 212601 (2017). DOI: 10.1063/1.4984134

[8] P.K. Day, H.G. LeDuc, B.A. Mazin, A. Vayonakis, J. Zmuidzinas. Nature, **425** (6960), 817 (2003).

[9] C.M. Natarajan, M.G. Tanner, R.H. Hadfield. Superconductor Sci. Technol., **25** (6), 063001 (2012).

[10] D.V. Reddy, R.R. Nerem, S.W. Nam, R.P. Mirin, V.B. Verma. Optica, **7** (12), 1649 (2020). DOI: 10.1364/OPTICA.400751

[11] J. Chang, J.W.N. Los, J.O. Tenorio-Pearl, N. Noordzij, R. Gourgues, A. Guardiani, J.R. Zichi, S.F. Pereira, H.P. Urbach, V. Zwiller, S.N. Dorenbos, I.E. Zadeh. APL Photonics, **6** (3), 036114 (2021). https://doi.org/10.1063/5.0039772

[12] W.-J. Zhang, J. Huang, Ch. Zhang, L.X. You, Ch. Lv, L. Zhang, H. Li, Zh. Wang, X. Xie. IEEE Transactions Appl. Supercond., **29** (5), 1 (2019). DOI: 10.1109/TASC.2019.2895621

[13] B. Korzh, Q. Zhao, J.P. Allmaras, S. Frasca, T.M. Autry, E.A. Bersin, A.D. Beyer, R.M. Briggs, B. Bumble, M. Colangelo, G.M. Crouch, A.E. Dane, Th. Gerrits, A. Lita, F. Marsili, G. Moody, C. Pena, E. Ramirez, J.D. Rezac, N. Sinclair, M. Stevens, A.E. Velasco, V. Verma, E.E. Wollman, S. Xie, D. Zhu, P.D. Hale, M. Spiropulu, K.L. Silverman, R.P. Mirin, S.W. Nam, A.G. Kozorezov, M.D. Shaw, K.K. Berggren. Nature Photon., **14** (4), 250 (2020).

[14] H. Shibata, K. Shimizu, H. Takesue, Y. Tokura. Opt. Lett., **40** (14), 3428 (2015). DOI: 10.1364/OL.40.003428

[15] D. Zhu, M. Colangelo, Ch. Chen, B.A. Korzh, F.N.C. Wong, M.D. Shaw, K.K. Berggren. Nano Lett., **20** (5), 3858 (2020).

[16] C. Cahall, K.L. Nicolich, N. Islam, G.P. Lafyatis, A.J. Miller, D. Gauthier J. Kim. Optica, **4** (12), 1534 (2017). DOI: 10.1364/OPTICA.4.001534

[17] Ch.M. Natarajan, L. Zhang, H. Coldenstrodt-Ronge, G. Donati, S.N. Dorenbos, V. Zwiller, I.A. Walmsley, R.H. Hadfield. Opt. Express, **21** (1), 893 (2013). DOI: 10.1364/OE.21.000893

[18] A. Divochiy, F. Marsili, D. Bitauld, A. Gaggero, R. Leoni, F. Mattioli, A. Korneev, V. Seleznev, N. Kaurova, O. Minaeva, G.N. Gol'tsman, K.G. Lagoudakis, M. Benkahoul, F. Levy, A. Fiore. Nature Photon., **2** (5), 302 (2008). DOI: 10.1038/nphoton.2008.95

[19] R. Cheng, H. Yin, J. Liu, T. Li, H. Cai, Z. Xu, W. Chen. IEEE Trans. Appl. Supercond., **23**, 2200309 (2013).

[20] F. Mattioli, Z. Zhou, A. Gaggero, R. Gaudio, R. Leoni, A. Fiore. Opt. Express, **24** (8), 9067 (2016). DOI: 10.1364/OE.24.009067

[21] E. Schmidt, E. Reutter, M. Schwartz, H. Vural, K. Ilin, M. Jetter, P. Michler, M. Siegel. IEEE Transactions Appl. Supercond., **29** (5), 1 (2019).

[22] E.E. Wollman, V.B. Verma, A.E. Lita, W.H. Farr, M.D. Shaw, R.P. Mirin, S.W. Nam. Opt. Express, **27** (24), 35279 (2019). DOI: 10.1364/OE.27.035279

[23] R. Cheng, Y. Zhou, S. Wang. M. Shen, T. Taher, H. Tang. Nat. Photon., **17**, 112 (2023). https://doi.org/10.1038/s41566-022-01119-3

[24] M. Schwartz, E. Schmidt, U. Rengstl, F. Hornung, S. Hepp, S.L. Portalupi, K. Ilin, M. Jetter, M. Siegel, P. Michler. Nano Lett., **18** (11), 6892 (2018).

[25] R.W. Klopfenstein. Proceed. IRE, **44** (1), 31 (1956).

[26] Q.Y. Zhao, D. Zhu, N. Calandri, A.E. Dane, A.N. McCaughan, F. Bellei, H.-Z. Wang, D.F. Santavicca, K.K. Berggren. Nature Photon., **11** (4), 247 (2017). DOI: 10.1038/nphoton.2017.35

Translated by E.Ilinskaya